

The Capacitance of Rosette Ice Crystals

MIHAI CHIRUTA AND PAO K. WANG

Department of Atmospheric and Oceanic Sciences, University of Wisconsin—Madison, Madison, Wisconsin

(Manuscript received 22 January 2002, in final form 24 October 2002)

ABSTRACT

The capacitances of seven bullet rosette ice crystals are computed based on the classical electrostatic analogy theory of diffusional growth. The rosettes simulated have 2, 3, 4, 6, 8, 12, and 16 lobes using mathematical formulas published previously. The Laplace equation for the water vapor density distribution around a stationary rosette is solved explicitly by the finite element method. The total flux of vapor toward the rosette surface and the vapor density on the surface determine the capacitance. The capacitances of these rosettes are smaller than that of spheres of equal radii but greater than columnar ice crystals of the same maximum dimensions. They can be greater or smaller than that of circular plates, depending on the number of lobes. Since many previous estimates of rosette growth rates were based on the assumption that their capacitances are the same as spheres of equal radii, the present finding implies that some of the previous rosette growth rates may be overestimated. The overestimation becomes less important if the rosettes have more lobes. Empirical power equations are given to fit the relations between the capacitance and the number of lobes, surface area, and volume of rosettes. Possible implications of rosette capacitance on the atmospheric heating by cirrus clouds are also discussed.

1. Introduction

It has recently become clear that cirrus clouds significantly affect the global energy balance and climate due to their great radiative impact on atmospheric thermal structure. Studies utilizing climate models are being conducted to understand the impact of cirrus on climate. In these types of studies it is necessary to assume certain radiative properties of cirrus clouds to assess their impacts. Variations in the assumed cirrus radiative properties can significantly alter the results of these climate models (Ramanathan et al. 1983; Liou 1992), and it is therefore important to formulate these properties correctly.

The radiative properties of a cirrus cloud depend on its microphysical properties such as ice crystal habit, ice water content, and number concentration. Recently, Liu (1999) and Liu et al. (2003a; Liu et al. 2003b, hereafter LWS) used a two-dimensional cirrus model to study the effects of cloud microphysical parameters on the cirrus development and found that both the cirrus development and its radiative property are sensitive functions of crystal habit. Their results indicate that, in addition to its direct impact on the scattering of radiation, the crystal habit may influence the overall cirrus radiative property via its control on the ice growth rate. During the diffusional growth process, ice crystals of

different habits may grow at different rates by vapor condensation. Thus, for example, even under the same initial and boundary conditions, a cirrus cloud consisting of columnar ice crystals may develop different ice concentration and ice water content than a cirrus consisting of ice plates. Such differences will result in different radiative properties.

In most cirrus models, the ice crystal growth rate is parameterized based on the classical ice growth theory, called the *electrostatic analogy* theory. In this theory, the diffusional growth rate of ice crystals depends on a quantity called *capacitance*, which is a function of both ice crystal size and habit. In order to determine the ice crystal growth rates in cirrus cloud models, it is necessary to know the values of the capacitance.

One of the most important ice crystal habits in cirrus is bullet rosettes (Heymsfield 1975; Parungo 1995). Heymsfield and Iaquinta (2000) reported high occurrence frequency of rosettes in midlatitude cirrus, making it one of the dominant habits for the cirrus clouds they have investigated. In view of this frequency, it is obviously important to have more accurate values of rosette capacitance in order to evaluate their growth rates and assess their impacts. Yet the capacitance of rosettes has never been determined rigorously, mainly due to their complicated shapes that render mathematical treatment difficult. To make some headway, McDonald (1963) and Heymsfield (1975) suggested that the capacitance of particles with more intricate and spatial branches, such as rosettes, could be approximated as that of spherical particles of equal radii. LWS used this

Corresponding author address: Dr. Pao K. Wang, Department of Atmospheric and Oceanic Sciences, University of Wisconsin—Madison, 1225 W. Dayton Street, Madison, WI 53706.
E-mail: pao@windy.meteor.wisc.edu

approximation to determine the growth rate of rosettes and showed that a cirrus cloud consisting of bullet rosettes would have much larger radiative effect than cirrus clouds of other ice crystal habits. Given the same initial environmental conditions, a peak heating rate due to infrared radiation for rosette cirrus, for cirrus ice columns and ice plates, and for spheres would be 2.5, 2, and 6 times greater, respectively. Its heating rate due to shortwave solar radiation is also substantially greater than other habits. Such a high potential impact on the atmospheric heating rates makes the determination of the bullet rosette capacitance even more urgent.

This paper is devoted to the task of calculating the capacitance of bullet rosette ice crystals. In the following sections, we will first review briefly the electrostatic analogy theory of ice crystal diffusional growth to clarify the role of the capacitance. Then we will describe the techniques of simulating the shapes of these rosettes and the methods of determining their capacitance. This will be followed by the discussion of the results and conclusions.

2. A brief review of the electrostatic analogy theory of ice crystal growth

The classical theory of ice crystal growth is called electrostatic analogy because it dwells on the similarity between the equations governing the water vapor distribution around an ice crystal and the electrostatic potential distribution around an electric conductor of the same shape as the ice crystal. A detailed discussion can be found in standard textbooks of cloud physics (e.g., Pruppacher and Klett 1997; Hobbs 1976; Young 1993). The following is a brief outline.

Note that the electrostatic analogy is only relevant to the growth of stationary ice crystals. Another important effect on the crystal growth, the ventilation effect that results from the motion of the crystal, requires the solutions of the Navier–Stokes equations for flow past rosette crystals, but unfortunately the solutions are not available at present.

The distribution of water vapor density ρ_v around a stationary ice crystal of arbitrary shape satisfies the Laplace equation

$$\nabla^2 \rho_v = 0, \quad (1)$$

with the following boundary conditions:

$$\rho_v = \begin{cases} \rho_s & \text{at the crystal's surface,} \\ \rho_\infty & \text{far away from the crystal,} \end{cases} \quad (2)$$

where both ρ_s and ρ_∞ are constant. In electrostatics, the electric potential φ around a conductor of the same (arbitrary) shape as the ice crystal would also satisfy the Laplace equation

$$\nabla^2 \varphi = 0, \quad (3)$$

with the boundary conditions

$$\varphi = \begin{cases} U & \text{on the crystal's surface,} \\ 0 & \text{at the outer boundary of the domain.} \end{cases} \quad (4)$$

Obviously, equation set (1) and (2) are completely equivalent to equation set (3) and (4), the only difference being the symbols. Thus, if the set (3) and (4) can be solved, the same solution would also satisfy the set (1) and (2). However, due to the complicated shapes of most ice crystals, we rarely solve these equations directly to determine the distributions of ρ_v and φ (although this was done in Ji and Wang 1999). Instead, since the main purpose of such calculations is to determine the ice crystal diffusional growth rate given by the integral

$$\frac{dm}{dt} = D_v \int_s \nabla \rho_v \cdot ds, \quad (5)$$

where m is the mass of the ice crystal, D_v the diffusivity of water vapor in air, and ds the infinitesimal increment of an arbitrary surface enclosing the ice crystal, it turns out that we can bypass the determination the explicit ρ_v distribution. This understanding stems from the well-known Gauss law in the classical electrostatics, which states that the enclosing surface integral of the electric flux density equals the total charge Q on the conductor.

On the other hand, the total charge Q is related to the electric potential by the following expression:

$$Q = C(U - 0) = CU, \quad (6)$$

where C is the capacitance of the conductor. Equation (6) is independent of the shape of the conductor. According to this analogy (see Pruppacher and Klett 1997 for details), the term dm/dt in (5) is analogous to Q and thus can be calculated by

$$\frac{dm}{dt} = 4\pi D_v C (\rho_\infty - \rho_s). \quad (7)$$

Equation (7) indicates that the growth rate of the ice crystal can be determined if its capacitance C is known. All other quantities on the right-hand side of (7) are independent of the shape.

The capacitance C in (7) can be either calculated or measured experimentally. While the capacitances of some simpler ice crystal shapes such as columns and plates have been theoretically calculated approximately or measured directly by using metal models of the crystals (McDonald 1963; Podzimek 1966; also see Pruppacher and Klett 1997, chapter 13), neither has ever been attempted for the important case of bullet rosettes. To our knowledge, the present study is the first to do so.

3. Mathematical determination of capacitance

a. Nondimensionalization of the governing equations

The main idea of determining the capacitance of a rosette is to utilize Eq. (7), namely, we shall determine dm/dt explicitly and then use (7) to obtain the capacitance C . This is analogous to determining the electric

capacitance of a conductor with known potentials on the surface and at infinity. To determine dm/dt , we need to explicitly solve the water vapor density distribution first. The governing equations for our problem are therefore Eq. (1), subject to appropriate boundary conditions.

The Laplace equation will be made dimensionless first for the convenience of analysis:

$$\nabla'^2 \rho'_v = 0, \quad (8)$$

where the primed quantity in the integrand are nondimensionalized according to the following relations:

$$\rho'_v = \frac{\rho_v - \rho_\infty}{\rho_s - \rho_\infty}, \quad \mathbf{r}' = \frac{\mathbf{r}}{a}, \quad (9)$$

where a is the radius of the ice crystal and \mathbf{r} the radial distance from the origin, which is defined at the center of the ice crystal in the present study. The radius of the rosette considered here is defined as the distance from the center of the rosette to the tip of one of the lobes. We assume that all lobes have the same length in this study.

Once the vapor density distribution ρ'_v is determined, the capacitance is obtained by

$$C = \frac{a}{4\pi} \oint_s \nabla' \rho'_v \cdot ds'. \quad (10)$$

Smythe (1956, 1962) and Wang et al. (1985) performed similar calculations to determine the capacitance of right circular cylinders of finite lengths by solving the Laplace equation analytically. In view of the more complicated rosette shape in the present study, we will use numerical techniques instead.

We need to carefully define appropriate boundary conditions for our numerical problem. Since the capacitance is a function of the position of these boundaries, the capacitance of an isolated conductor will be different from the same conductor when it is placed near another charged body with a certain potential. This means that the distance of the outer boundary may have an effect on the precise value of the capacitance. In atmospheric clouds, the mean distance between individual cloud particles is rather large relative to the particle size, typically on the order of many tens to hundreds of particle radii (Pruppacher and Klett 1997). Thus the ice particles can often be considered as isolated individual particles, and hence the most relevant capacitance for our purpose here will be that of an isolated ice crystal; that is, the outer boundary should be placed at infinity. Thus boundary condition (2) is appropriate. In numerical calculations, the term ‘‘infinity’’ is replaced by ‘‘sufficiently far away.’’ In nondimensional form, the appropriate boundary conditions for the present situation are

$$\rho'_v = \begin{cases} 1 & \text{on the surface of the rosette,} \\ 0 & \text{at a distance far away from the rosette.} \end{cases} \quad (11)$$

b. Treatment of the boundary conditions

1) THE INNER BOUNDARY

We will use the finite element techniques to solve the Laplace equation (8) subject to the boundary conditions (11). This requires setting up a grid system for the computational domain between the inner and outer boundaries. The first step for this analysis is to prescribe the boundary points.

The inner boundary is the surface of the bullet rosette. The shape of a bullet rosette is highly complicated, and it is not easy to determine the coordinates of the boundary surface. To simplify this problem, we use the successive modification of simple shapes (SMOSS) technique developed by Wang (1997, 1999, 2002) to simulate the shape of ice crystals. The mathematical expression specific for this case is given in Wang (1999):

$$r = \{\alpha[\cos^2(m\theta)]^\beta + \gamma\}^\delta \{\alpha'[\sin^2(n\varphi)]^{\beta'} + \gamma'\}^{\delta'}. \quad (12)$$

This equation is expressed in spherical coordinates so that r is the radial, θ the zenithal, and φ the azimuthal coordinates. The parameters α , β , γ , δ , α' , β' , γ' , and δ' are freely adjustable in order to fit the shape of a particular rosette. The shape generated by this expression will have $2mn$ lobes or branches. For example, a four-branch combination of bullets can be generated by the following expression:

$$r = [1 - \cos(2\theta)^4]^{20} [1 - \sin(\varphi)^4]^{20}, \quad (13)$$

where $m = 2$ and $n = 1$ here. The width of the branch is controlled by β and β' in (12). Obviously, it is impossible that such a simple expression will reproduce all the intricate structures, but at least it captures the essential multilobe feature that is characteristic of bullet rosette crystals.

2) THE OUTER BOUNDARY

Although the inner boundary of the problem is not spherically symmetric, the outer boundary of the present problem, if set at infinity, will be a sphere, as the distribution of any field whose source is finite (such as the rosette considered here) will become spherically symmetric when the distance approaches infinity. However, in numerical calculations, the distance of the outer boundary from the origin has to remain finite and hence the field distribution here may deviate from being truly spherically symmetric. In the present study, we assume that this finite outer boundary surface is also spherical. In order to assess the impact of this assumption on the accuracy of the results, we performed tests to determine how sensitive the results are to the outer boundary distance. It turns out that the results are not very sensitive to the outer boundary distance as long as it is at least seven radii away from the center of the crystal. Further

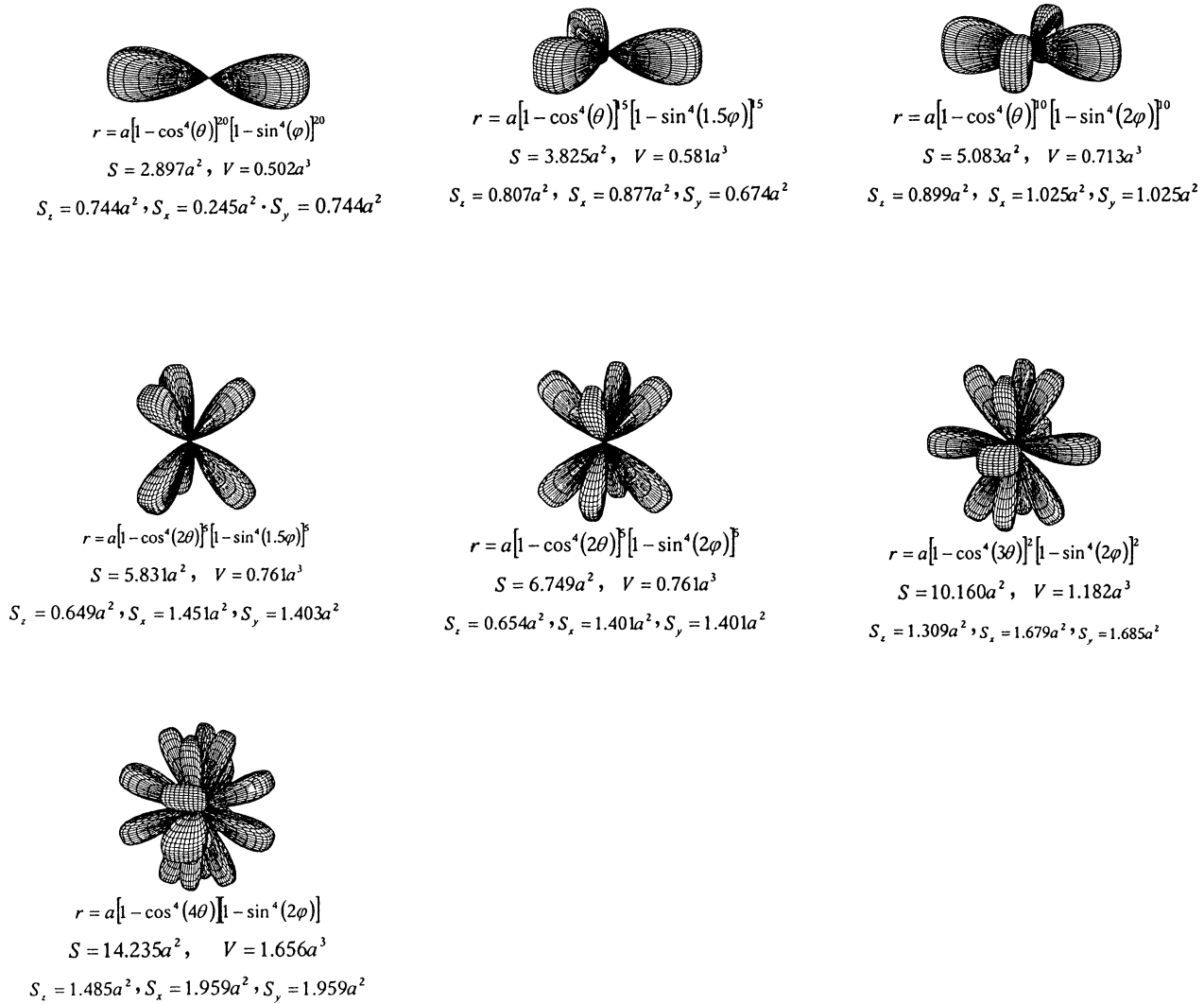


FIG. 1. The seven simulated bullet rosette ice crystals and their generating equations, surface area (S), volume (V), and the projected areas in x , y , and z direction. The areas are in units of a^2 , and the volume in a^3 .

discussion on the sensitivity tests will be included in the next section.

A brief description of the discretization techniques used for the present study and an example of the grid structure are given in the appendix.

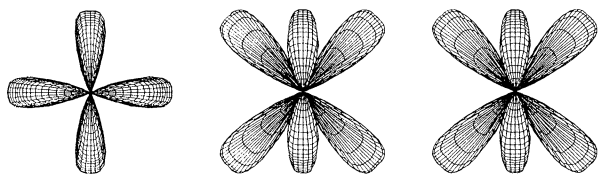
4. Results and discussion

The capacitances of seven bullets rosette crystals are calculated using the techniques outlined in the previous section. These rosettes have 2, 3, 4, 6, 8, 12, and 16 lobes. These rosette cases are chosen because their geometrical symmetries render them easier for mathematical treatment. The mathematical expressions for the rosettes and plots of their shapes are shown in Fig. 1. The rosettes look visually reasonable when compared with photographs of actual samples. More quantitative discussions of their geometrical properties are given in

the next section. Due to the limitation of the formulas, it is sometimes difficult to obtain a completely symmetric shape for individual lobes. Thus sometimes the dimension of a lobe in θ direction is substantially different than that in φ direction. But the multilobe characteristic of the rosettes is well reproduced. The crystals generated in this way have the lobes of equal length a . Also included in Fig. 1 are values of the rosettes' total surface areas, volumes, and the cross-sectional areas S_x , S_y , and S_z projected in the x , y , and z axis, respectively. As an example, Fig. 2 shows plots of the projected cross-sectional areas of an eight-lobed rosette.

a. Geometrical properties of the modeled rosettes

It is useful to briefly mention some geometrical properties of the modeled rosettes. Figure 3 shows the variation of the rosettes' surface areas and volumes with



$$S_z = 0.654a^2 \quad S_x = 1.401a^2 \quad S_y = 1.401a^2$$

FIG. 2. The projected areas S_x , S_y , and S_z of an eight-lobed bullet rosette simulated in the study.

the number of lobes. It appears that while both the surface area and volume increase with the number of lobes, the increasing rates are not uniform that may be due to the specific set of parameter values used. The solid curves represent power fit by the following formulas:

$$A = 1.5528N^{0.7727}a^2 \quad (\text{surface area}) \quad \text{and} \\ V = 0.3257N^{0.5206}a^3 \quad (\text{volume}). \quad (14)$$

Higher-order polynomials can fit even closer, but we feel it is unnecessary.

Figures 4 and 5 show the plots of the surface area and volume versus the radius as computed from (14) for all seven-rosette cases. It is seen that the surface areas of all rosettes, except the 16-lobed ones, are smaller than that of a sphere of equal radius. On the other hand, the sphere volume is always greater than the volume of a rosette regardless of the number of lobes. Naturally, as the number of rosette lobes increases, the volume increases also.

Heymsfield and Iaquinta (2000) presented some observational results of bullet rosettes in cirrus clouds, and it is useful to compare their geometrical properties with the simulated models in this study. Since the models used in this study are dimensionless, the most convenient

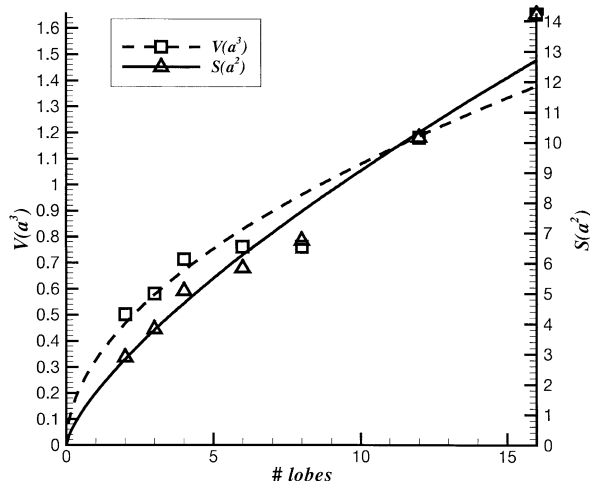


FIG. 3. Variation of the surface area and volume of the simulated rosettes as a function of number of lobes.

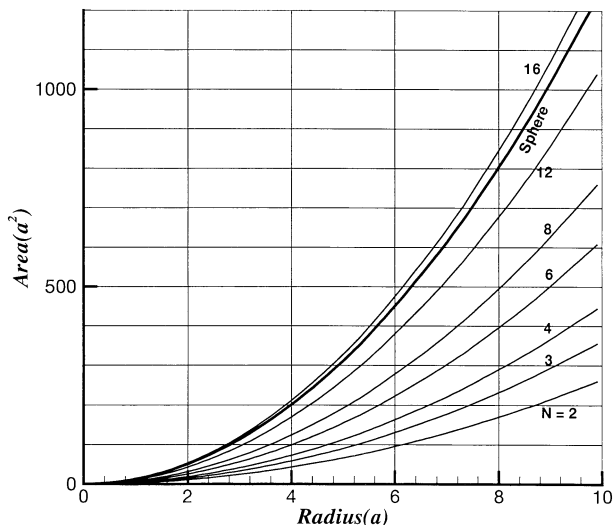


FIG. 4. Variation of surface area vs radius of rosettes. Here N represents the number of lobes of the rosette. The thick curve is for spheres.

parameter for comparing the geometrical properties is the aspect ratio, defined as the width w divided by the length L of a bullet.

To determine the aspect ratio of the seven rosettes we used the maximum width of the lobe as the width of the bullet. The length L is of course equal to a of the lobe. The aspect ratios of the modeled rosettes, so determined, vary between $0.35 \sim 0.6$. Those with fewer lobes are usually associated with larger aspect ratios and those with more lobes are associated with smaller aspect ratios, but the relation is not monotonic. This range of aspect ratios appears to be consistent with the majority of the bullet rosettes observed by Heymsfield and Iaquinta (2000).

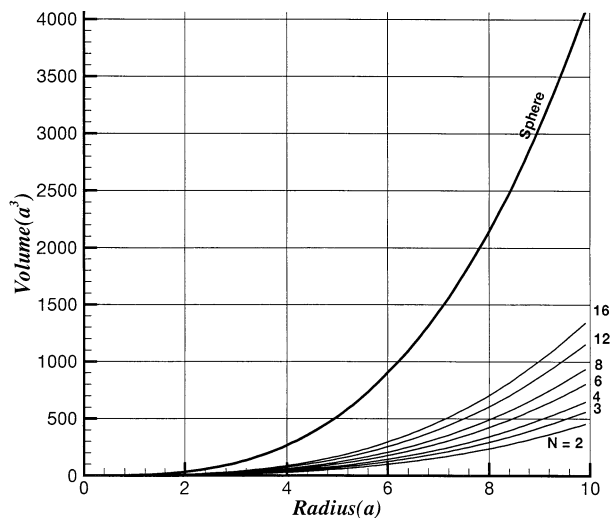


FIG. 5. Variation of volume vs radius of rosettes. Here N represents the number of lobes of the rosette. The thick curve is for spheres.

The volume of a bullet rosette calculated using (14) is also generally consistent with that calculated using the empirical formula given by Heymsfield and Iaquinta. For example, the volume of a five-lobed rosette calculated from (14) will be the same ($\sim 0.75 a^3$) as that calculated using their Eq. (A10) if the aspect ratio is taken to be 0.45. It is noted that (14) does not include the aspect ratio effect, hence the volume calculated by it will be different from Heymsfield and Iaquinta's formula if the aspect ratio changes.

Yang et al. (2000) also suggested a few empirical parameters to characterize the geometrical properties of nonspherical ice particles including rosettes. Their main purpose was for the parameterization of scattering and absorption properties of these particles. One of the parameters they suggested is the equivalent radius d_e defined as $1.5 (V/A)$, where V is the volume and A the projected area. The four- and six-lobed rosettes modeled in the present study resemble that described in Yang et al. (2000) and have d_e varying with a in a similar manner, but the values are larger for the same maximum dimension. The differences are smaller when rosettes are small but become much larger when rosettes reach millimeter size. More research is needed to understand the significance of such differences.

b. Capacitances of rosettes

Since both the grid resolution and the distance of outer boundary may influence the precision of the results, we performed several sensitivity tests in order to ensure the accuracy of the computed capacitances. The first test is on the sensitivity of grid resolution. Several grids were set up for the solutions of ρ'_v in (8) and the results compared. If the results are similar (less than about 5% difference), the one with the least resolution is adopted as the grid for the calculations to achieve computational efficiency.

The second test is on the sensitivity of the distance of the outer boundary. This distance was set at different values from 2.5 to 15 and the respective capacitance was computed accordingly. As an example, the computed capacitances of an eight-lobed rosette with different outer boundary distances are shown in Fig. 6. We see in Fig. 6 that as the distance of the outer boundary b increases, the capacitance of the rosette decreases and approaches an asymptotic value. This asymptotic value should represent the capacitance of an isolated rosette (i.e., when the outer boundary is set at infinity) and is the value reported here. As mentioned before, the capacitance becomes more or less constant for outer boundary distance greater than ~ 6 radii.

To determine the capacitance, the numerical solutions of ρ'_v are fed into Eq. (10) and the integral is computed numerically. In an exact analytical theory, the results of integration is independent of the surface chosen because of the steady-state condition implied in the formulation, but in numerical calculations these results may be some-

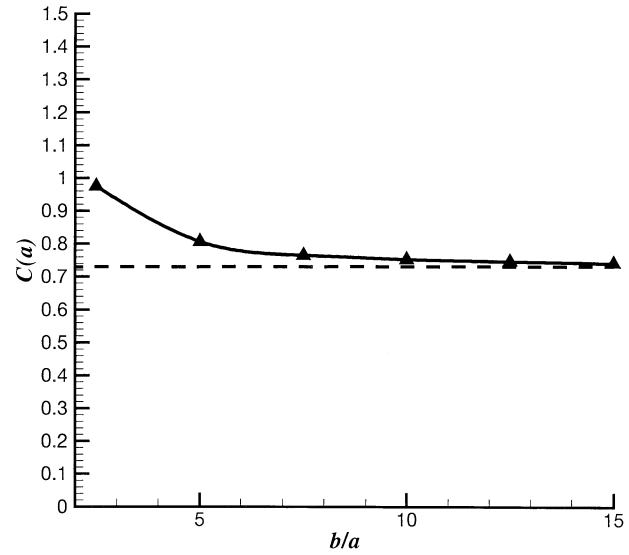


FIG. 6. The computed capacitance of an eight-lobed rosette as a function of the outer boundary distance.

what different due to numerical errors in the solutions of ρ'_v . In order to ensure accuracy, we performed the integration in (10) over 10 different surfaces to make sure that errors are insignificant. It turned out that the differences are typically less than 5%, thus an averaged value of all of these results should be representative of the true value of the capacitance.

The computed capacitances of the rosettes as a function of the number of lobes are shown in Fig. 7. The slight scatter in the results is largely due to the shape parameters chosen in Eq. (12). However, the general trend of the curve is fairly clear and the scatter should not influence the conclusions to any significant extent.

It is seen in Fig. 7 that the rosette capacitance increases from about 0.5 to near 0.9 (in unit of a) as the number of lobes increases from 2 to 16. The capacitance of a conducting sphere is its radius a . Thus it appears that the capacitance of a rosette will approach that of a sphere if the number of lobes approaches infinity, that is, as its shape approaches a sphere. The following power relation can fit the rosette capacitance curve in Fig. 7:

$$C = 0.434N^{0.257}, \quad (15)$$

where C is the capacitance in unit of a and N is the number of lobes.

Figure 7 thus shows that the capacitance of a rosette is smaller than that of a sphere of equal radius. This implies that calculations of the rosette growth rate based on the spherical capacitance assumption overestimate. The overestimation is the most serious for rosettes with fewer lobes but becomes less if the number of lobes is large.

The capacitances of a thin circular plate and two cases of prolate spheroids are also shown in Fig. 7 for comparison. These shapes have been used previously as ap-

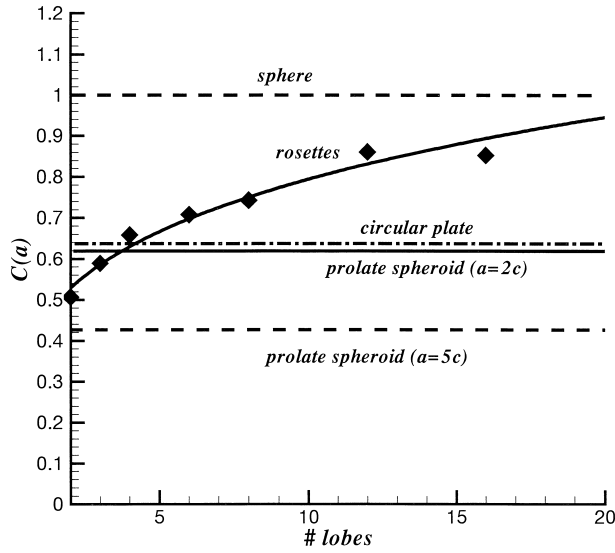


FIG. 7. Computed capacitance (diamonds) of rosettes as a function of number of lobes. Thick solid curve represent power fit by Eq. (15). Also shown are the capacitances of a sphere (thin solid line), a circular plate (dashed), and two prolate spheroids with semi-axis ratio $a/b = 2$ and 5 , respectively. The rosettes, the sphere, and circular plate all have a radius a .

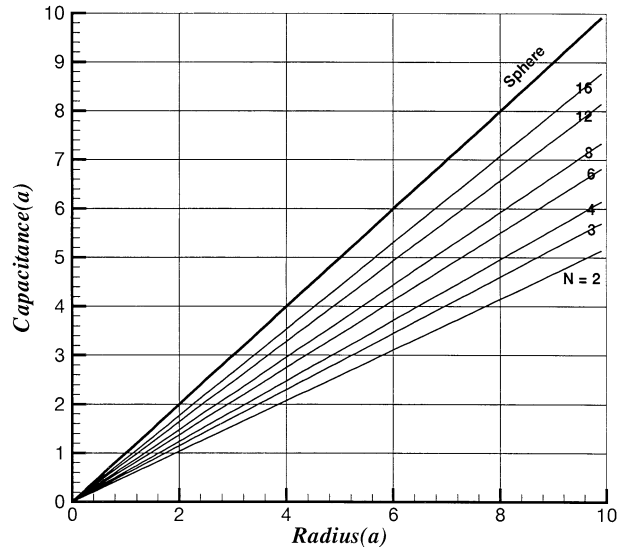


FIG. 8. Variation of capacitance with radius of rosettes calculated using (15). Here N represents the number of lobes of the rosette. The thick curve is for spheres.

proximations for ice plates and ice columns and their capacitance formulas are given as

$$C = \frac{2a}{\pi} \quad (\text{circular plate}) \quad \text{and}$$

$$C = \frac{\sqrt{a^2 - c^2}}{\ln(2a/c)} \quad (\text{prolate spheroid}), \quad (16)$$

where a and c in the second equation represent the semimajor and semiminor axes of the prolate spheroid, respectively (see Pruppacher and Klett 1997, chapter 13, p. 548). Note that the semilength (the longer dimension) instead of the radius of the prolate spheroid is denoted as a . McDonald (1963) and Podzimek (1966) performed laboratory measurements of the capacitances of metal models of ice columns, plates, and dendrites, and their results are close to that given by Eq. (16), usually to about 10% or less. Only the highly skeleton stellar crystal [P1d in Magono–Lee classification, see Magono and Lee (1966)] has a capacitance about 23% less than that given by the plate in (16). Hence the capacitances given by (16) are fairly representative of the atmospheric ice crystals.

We will use the capacitance of a prolate spheroid to approximate that of a hexagonal column in the following discussion. We see that the capacitance of a two-lobed rosette crystal is smaller than that of a short column ($a = 2c$) ($C \sim 0.65$) but is greater than that of a long thin column ($a = 5c$). A five-lobed rosette has a capacitance close to that of a short column. This implies that the growth rate of a rosette ice crystal is usually greater

than that of a long thin column and may even be greater than a short column if it has more than five lobes.

The capacitance of a circular plate is greater than that of rosettes of the same radii up to five lobes, but becomes smaller than rosette capacitance as the number of rosette lobes increases. If the rosette has more than five lobes, its growth rate will be faster than an ice plate of the same dimension.

Figure 8 shows the plot of capacitance versus radius for rosettes as computed using (15). The case of spheres is also given here for comparison.

Since the surface area and volume of a rosette are important geometrical properties, it is useful to examine the relations between the capacitance and these two geometrical quantities. Figures 9 and 10 show the variation of the capacitance with rosette surface area and volume. The capacitance of the rosettes generally increases with increasing surface area and volume. The curves represent the power fits

$$C = 0.3636S^{0.3476} \quad (\text{surface area}) \quad \text{and}$$

$$C = 0.7472V^{0.4401} \quad (\text{volume}). \quad (17)$$

It is of interest to compare the capacitances between rosettes and spheres of equal areas and volumes. To do so, we used (14) to calculate the areas and volumes of the rosettes and (15) to calculate the capacitances for a given N . Figure 11 shows the comparison for equal areas. It is seen that rosettes have capacitances larger than a sphere of equal area if the number of lobes is smaller than ~ 6 . For a rosette with more than six lobes, the capacitance becomes smaller than that of a sphere of equal area, and the more lobes it has, the smaller the capacitance becomes. One factor that contributes to this

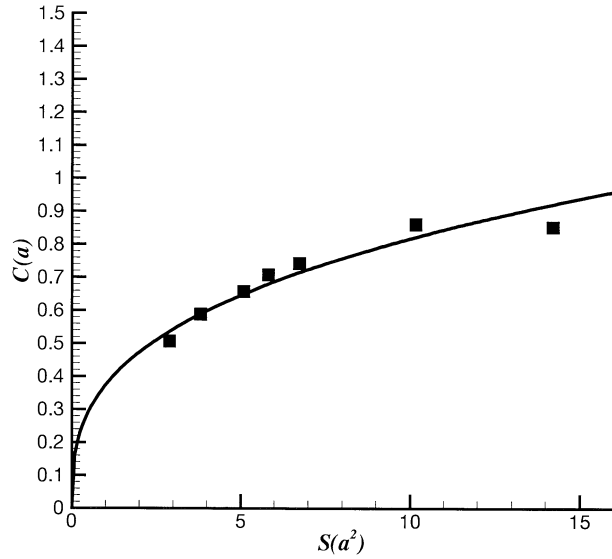


FIG. 9. Computed rosette capacitance (squares) as a function of rosette surface area. The solid curve represents power fit by Eq. (17).

behavior is the linear dimension of rosettes. A rosette with few lobes needs to be substantially longer than a sphere in order to have same area. Such a long rosette tends to have higher capacitance than the sphere. On the other hand, a rosette with more lobes need not be much longer than a sphere to have the same area. Figure 4 shows that, as the number of lobes increases the rosettes modeled here, the surface area of a rosette becomes closer to that of a sphere of equal radius. A rosette with 16 lobes even has an area greater than a sphere of equal radius. Of course, the linear dimension is not the only factor deciding the capacitance and other factors

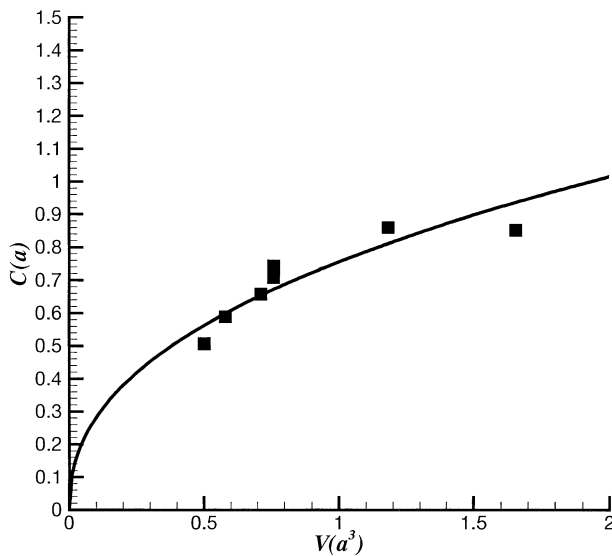


FIG. 10. Computed rosette capacitance (squares) as a function of rosette volume. The solid curve represents power fit by Eq. (17).

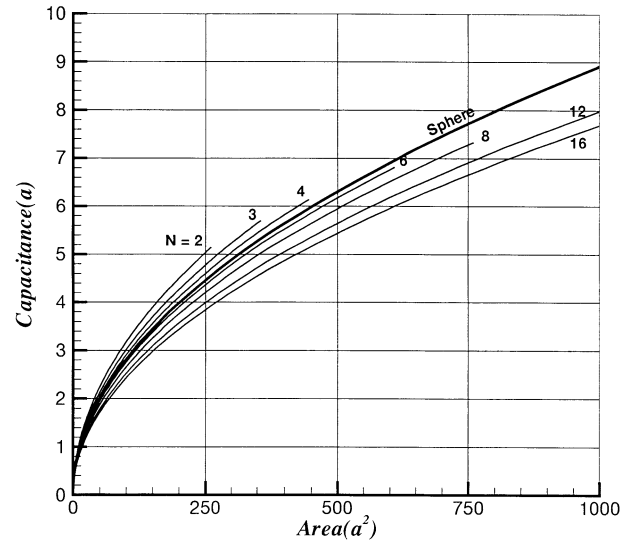


FIG. 11. Variation of capacitance with rosette surface area. Here N represents the number of lobes of the rosette. The thick curve is for spheres.

should be considered to fully understand the behavior of the curves in Fig. 11.

The comparison for equal volume is given in Fig. 12, which shows that the capacitances of rosettes are greater than a sphere of equal volume in all cases, and the more the lobes, the greater the capacitance. More studies are being conducted to understand this phenomenon.

Since equal volume means equal amount of water content, Fig. 12 implies that, given the same amount of water substance and holding other environmental conditions constant, a cirrus cloud composed of bullet ro-

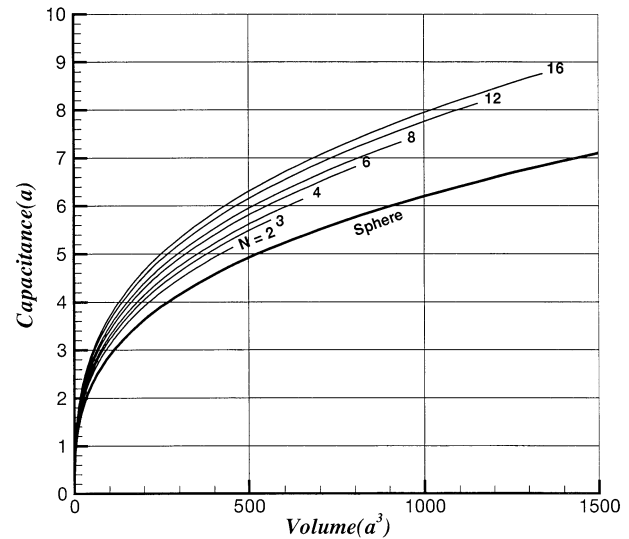


FIG. 12. Variation of capacitance with rosette volume. Here N represents the number of lobes of the rosette. The thick curve is for spheres.

settes will grow more vigorously than one composed of spheres (e.g., frozen drops). In addition, the more lobes the rosettes have, the faster they will grow. Such rapid growth rates would imply greater impact on the cloud heating of the atmosphere. This is one of the main conclusions of LWS's study and suggests that the impact of ice habit, especially that of rosettes, on the cirrus development has to be assessed carefully.

Finally, it is known that rosettes can consist of hollow bullets, which are not represented by Eq. (12) and whose capacitances may differ from that given above. More research is needed to determine the capacitance of such hollow rosettes.

5. Conclusions

Heymsfield and Platt (1984), Heymsfield and McFarquhar (1996, 2002), McFarquhar and Heymsfield (1996), and Heymsfield and Iaquinta (2000) indicated that ice columns and bullet rosettes dominate the mid-latitude cirrus, so it is meaningful to compare the capacitances of these two ice habits. The results presented above show that those rosettes with five lobes have capacitances closer to that of ice columns of similar maximum dimensions, but those with more lobes would have capacitances much greater than columns. The rosette capacitances, even those with few lobes, are greater than long, thin columns. Since the growth rate is directly proportional to the capacitance, this implies that rosettes will, in general, grow much faster than columns. On the other hand, the assumption that a rosette will have capacitance of a sphere of equal radius would overestimate the growth rate. The magnitude of overestimation would depend on the number of lobes of the rosette in question.

Observations suggest that the dominant number of rosette lobes is either about 3 ~ 4 (Kikuchi 1968) or 5 (Heymsfield and Iaquinta 2000; A.J. Heymsfield 2001, personal communication). In either case, the capacitance of rosettes will definitely be greater than the columns (more than 2 times larger than the long thin columns) but smaller than the spheres of the same maximum dimensions. Since the growth rate is directly proportional to the capacitance, an accurate assessment of the rosette growth rate in a particular cirrus cloud seems to hinge upon a good estimate of their mean number of lobes.

The rosette growth rate estimates based on the new capacitance results will certainly impact on the development of cirrus clouds and thence the heating rates of the atmosphere caused by the presence of cirrus. But due to the complexity in the interaction between cloud dynamics and microphysics, we need to use a realistic cirrus model to assess these impacts.

Acknowledgments. We thank A. Heymsfield for information about the geometrical properties of the bullet rosettes in cirrus. P. Yang and two anonymous reviewers also gave helpful comments that result in improvements

of the paper. This work is supported by the NSF Grant ATM-9907761.

APPENDIX

Finite Element Techniques Used for the Present Study

This appendix provides a brief summary of the discretization technique used for numerically solving the Laplace equation for the water vapor density and the equations that give the Cartesian components of the water vapor flux density. The specific discretization technique we used is the finite element analysis and readers are referred to standard textbooks for a general discussion (see, e.g., Fletcher 1984). Since the discussions of finite element methods in most textbooks are confined to two-dimensional cases whereas the present application is three-dimensional, we feel it is useful to provide some details.

The finite elements chosen for the present study were tetrahedrons. We used quadratic functions for the water vapor density and linear functions for the flux density components for interpolation purpose. This combination of interpolation functions ensures a continuous water vapor flux density profile. The water vapor flux density continuity allows small numerical errors in the capacitance using a reasonable discretization of the analysis domain.

The water vapor density approximation on a tetrahedron is given by

$$\hat{\rho}_v = \sum_{i=1}^{10} N_i \rho_{vi}, \quad (\text{A1})$$

where N_i s are the quadratic interpolation functions (Dawe 1987) and ρ_{vi} are the values of the water vapor density at the vertices and midpoints of edges of the tetrahedron.

Since $\hat{\rho}_v$ is an approximation of the exact solution, it does not satisfy the Laplace equation and hence we have a residual $R(x, y, z, N_i)$:

$$\frac{\partial^2 \hat{\rho}_v}{\partial x^2} + \frac{\partial^2 \hat{\rho}_v}{\partial y^2} + \frac{\partial^2 \hat{\rho}_v}{\partial z^2} = R(x, y, z, N_i). \quad (\text{A2})$$

The application of the weighted residual method (Fletcher 1984) to minimize the residual term leads to the following elemental algebraic equation:

$$\mathbf{A}^e \hat{\rho}_v = 0, \quad (\text{A3})$$

with the components of the \mathbf{A}^e matrix being

$$A_{ij}^e = \int_{V_e} \left(\frac{\partial N_i}{\partial x} \frac{\partial N_j}{\partial x} + \frac{\partial N_i}{\partial y} \frac{\partial N_j}{\partial y} + \frac{\partial N_i}{\partial z} \frac{\partial N_j}{\partial z} \right) \hat{\rho}_{vj} dV, \quad (\text{A4})$$

where the integral is calculated over the volume of the finite element.

The elemental equations are assembled over the whole analysis domain in accordance with the topology

of the discretization. This forms an algebraic system of equations whose solutions are the values of the water vapor density at the nodes of the discretization.

The approximate value of the x component of water vapor flux density in polynomial form is given by

$$\hat{j}_x = \sum_{i=1}^4 L_i j_{xi}, \quad (\text{A5})$$

where L_i s are the linear interpolation functions given in Dawe (1987) and j_{xi} s are the values of the x component of vapor density flux in the tetrahedron vertices.

Using the approximate value of the water vapor density $\hat{\rho}_v$, the x component of vapor flux density can be written as

$$\hat{j}_x = -\frac{1}{D} \frac{\partial \hat{\rho}_v}{\partial x}. \quad (\text{A6})$$

Using the weighted residual method described previously, we obtain the elemental equations for the x component of vapor flux density

$$\mathbf{B}^e \hat{j}_x^e = -\mathbf{f}_x^e, \quad (\text{A7})$$

where the components of the matrix \mathbf{B}^e are

$$B_{ij}^e = \int_{V_e} L_i L_j dV, \quad (\text{A8})$$

and those of the matrix \mathbf{f}_x^e are

$$f_{xi}^e = \frac{1}{D} \int_{V_e} L_i \left(\sum_{j=1}^{10} \frac{\partial N_j}{\partial x} \hat{\rho}_{vj} \right) dV. \quad (\text{A9})$$

Assembling the elemental equations (A7) over the whole domain, we again obtain a system of algebraic

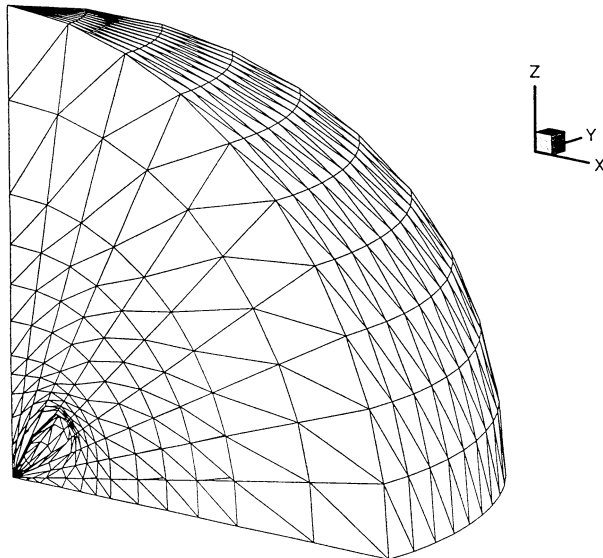


FIG. A1. The discretization into finite elements of the analysis domain for an eight-lobed bullet rosette ice crystal. The length of a lobe is a and the radius of the outer sphere is $b = 5 \times a$.

equations whose solutions are the x component values of vapor flux density at the nodes of the discretization. The y and z components of vapor flux density are obtained in a similar fashion.

In the initial formulation as described in section 2, the inner boundary of the domain is the rosette surface and the outer boundary is a sphere with radius b , centered at the center of the crystal. In actual calculations we only need to use a portion of this domain because of the symmetry of the rosettes. However, this results in new boundary surfaces when we cut the original domain into separate portions (see Fig. A1). It is therefore necessary to specify the conditions in these new surfaces. Here we use the requirement that the normal derivative of the water vapor density be zero as the boundary conditions.

REFERENCES

- Dawe, D. J., 1987: Curved beam and arch elements. *Finite Element Handbook*, H. Kardestuncer, Ed., McGraw-Hill, 2.128–2.129.
- Fletcher, C. A. J., 1984: *Computational Galerkin Methods*. Springer, 300 pp.
- Heymsfield, A. J., 1975: Cirrus uncinus generating cells and the evolution of cirroform clouds. III. *J. Atmos. Sci.*, **32**, 799–808.
- , and C. M. R. Platt, 1984: A parameterization of the particle size spectrum of ice clouds in terms of the ambient temperature and ice water content. *J. Atmos. Sci.*, **41**, 846–855.
- , and G. M. McFarquhar, 1996: High albedos of cirrus in the tropical Pacific warm pool: Microphysical interpretations from CEPEX and from Kwajalein, Marshall Islands. *J. Atmos. Sci.*, **53**, 2424–2451.
- , and J. Jaquinta, 2000: Cirrus crystal terminal velocities. *J. Atmos. Sci.*, **57**, 914–936.
- , and G. M. McFarquhar, 2002: Mid-latitude and tropical cirrus microphysical properties. *Cirrus*. D. Lynch, Ed., Oxford University Press, 288 pp.
- Hobbs, P. V., 1976: *Ice Physics*. Oxford University Press, 837 pp.
- Ji, W., and P. K. Wang, 1999: Ventilation coefficients of falling ice crystals at low–intermediate Reynolds numbers. *J. Atmos. Sci.*, **56**, 829–836.
- Kikuchi, K., 1968: On snow crystals of bullet type. *J. Meteor. Soc. Japan*, **46**, 128–132.
- Liou, K. N., 1992: *Radiation and Cloud Processes in the Atmosphere*. Oxford University Press, 487 pp.
- Liu, H. C., 1999: A numerical study of cirrus clouds. Ph.D. thesis, Dept. of Atmospheric and Oceanic Sciences, University of Wisconsin—Madison, 257 pp.
- , P. K. Wang, and R. E. Schlesinger, 2003a: A numerical study of cirrus clouds. Part I: Model description. *J. Atmos. Sci.*, in press.
- , —, and —, 2003b: A numerical study of cirrus clouds. Part II: Effects of ambient temperature, stability, radiation, ice microphysics and microdynamics on cirrus evolution. *J. Atmos. Sci.*, in press.
- Magono, C., and C. W. Lee, 1966: Meteorological classification of natural snow crystals. *J. Fac. Sci. Hokkaido University, Ser. VII*, **2**, 321–335.
- McDonald, J. E., 1963: Use of electrostatic analogy in studies of ice crystal growth. *Z. Angew. Math. Phys.*, **14**, 610.
- McFarquhar, G. M., and A. Heymsfield, 1996: Microphysical characteristics of three anvils sampled during the Central Equatorial Pacific Experiment. *J. Atmos. Sci.*, **53**, 2401–2423.
- Parungo, F., 1995: Ice crystals in high clouds and contrails. *Atmos. Res.*, **38**, 249–262.

- Podzimek, J., 1966: Experimental determination of the "capacity" of ice crystals. *Studia Geophys. Geodet.*, **10**, 235–238.
- Pruppacher, H. R., and J. D. Klett, 1997: *Microphysics of Clouds and Precipitation*. Kluwer Academic, 954 pp.
- Ramanathan, V., E. J. Pitcher, R. C. Malone, and M. L. Blackmon, 1983: The response of a spectral general circulation model to refinements in radiative processes. *J. Atmos. Sci.*, **40**, 605–630.
- Smythe, W. R., 1956: Charged right circular cylinders. *J. Appl. Phys.*, **27**, 917–920.
- , 1962: Charged right circular cylinders. *J. Appl. Phys.*, **33**, 2966–2967.
- Wang, P. K., 1997: Characterization of ice particles in clouds by simple mathematical expressions based on successive modification of simple shapes. *J. Atmos. Sci.*, **54**, 2035–2041.
- , 1999: Three-dimensional representations of hexagonal ice crystals and hail particles of elliptical cross sections. *J. Atmos. Sci.*, **56**, 1089–1093.
- , 2002: *Ice Microdynamics*. Academic Press, 273 pp.
- , C. H. Chuang, and N. L. Miller, 1985: Electrostatic, thermal and vapor density fields surrounding stationary columnar ice crystals. *J. Atmos. Sci.*, **42**, 2371–2379.
- Yang, P., K. N. Liou, K. Wyser, and D. Mitchell, 2000: Parameterization of the scattering and absorption properties of individual ice crystals. *J. Geophys. Res.*, **105**, 4699–4718.
- Young, K. C., 1993: *Microphysical Processes in Clouds*. Oxford University Press, 427 pp.